

NASA Technical Memorandum 102284  
AIAA-89-2723

# The Effects of Arcjet Operating Condition and Constrictor Geometry on the Plasma Plume

Lynnette M. Carney  
*Lewis Research Center*  
*Cleveland, Ohio*

and

John M. Sankovic  
*The University of Akron*  
*Akron, Ohio*

(NASA-TM-102284) THE EFFECTS OF ARCJET  
OPERATING CONDITION AND CONSTRICTOR GEOMETRY  
ON THE PLASMA PLUME (NASA. Lewis Research  
Center) 29 P CSCI 21H

N89-25281

Unclas  
G3/20 0217632

Prepared for the  
25th Joint Propulsion Conference  
cosponsored by the AIAA, ASME, SAE, and ASEE  
Monterey, California, July 10-12, 1989

**NASA**

# THE EFFECTS OF ARCJET THRUSTER OPERATING CONDITION AND CONSTRICTOR GEOMETRY ON THE PLASMA PLUME

Lynnette M. Carney  
National Aeronautics and Space Administration  
Lewis Research Center  
Cleveland, OH 44135  
and  
John M. Sankovic  
The University of Akron  
Akron, OH 44325

## ABSTRACT

Measurements of plasma number density and electron temperature have been obtained in the plumes of laboratory arcjet thrusters using electrostatic probes of both spherical and cylindrical geometry. The two arcjet thrusters used in this investigation had different constrictor/nozzle geometries and operated on mixtures of nitrogen, hydrogen, and ammonia to simulate the decomposition products of hydrazine and ammonia. An increase in the measured electron number density was observed for both geometries with increasing arc power at a constant mass flow rate and with increasing mass flow rate at a constant arc current. For a given operating condition, the electron number density decreased exponentially off centerline and followed an inverse distance-squared relationship along the thrust axis. Typical measured electron temperatures ranged from 0.1 to 0.2 eV.

## INTRODUCTION

The low power arcjet thruster is under development for auxiliary propulsion applications such as north-south stationkeeping onboard communications satellites.<sup>1,2</sup> As the arcjet thruster moves closer to being a flight ready propulsion system, spacecraft integration concerns become of significant interest. One key issue centers on the potential impact that the arcjet plume may have on the transmission of RF signals in common use for satellite communications. A first order study<sup>3</sup> evaluated the interaction between a 1 kW arcjet plume and a 4 GHz communications signal in terms of signal attenuation and phase shift between transmitting and receiving antennas. In the antenna far field, the impacts appear negligible, except for propagation paths which pass very near the arcjet source. Numerical techniques are necessary to fully define the interaction processes and effects which would occur if the plasma were to expand within the antenna near field. Other integration concerns focusing on plume impacts include thermal loading and thrust losses due to impingement, particle contamination, and electromagnetic interference (EMI).

A complete assessment of the potential plume impacts requires a detailed characterization of the arcjet exhaust. Initial research efforts<sup>4</sup> demonstrated the applicability of Langmuir probes for the measurement of arcjet plasma properties and provided a partial description of the arcjet exhaust. Measurements 30 cm downstream of the thruster exit plane indicated plasma number densities on the order of  $5 \times 10^9 \text{ cm}^{-3}$  at electron temperatures between 0.4 and 0.8 eV. The exhaust was only slightly ionized (much less than one percent). An increase in measured number density was observed with increasing arc current at a constant mass flow rate and also with an increasing mass flow rate at constant current. Radial measurements 18 cm downstream of the thruster exit plane indicated that the plasma number density decreased exponentially as a function of angle off centerline while values of electron temperature remained relatively constant with position. Similarly, an axial survey along plume centerline revealed plasma number density decreases as the inverse distance-squared. Finally, the initial study demonstrated an uncertainty in the true collection area of a spherical probe in a flowing plasma due to wake effects.

This paper extends the previous work and presents a body of experimental data which correlate measured plasma properties in the arcjet plume with thruster operating conditions for two different constrictor/nozzle

geometries. The Langmuir probe is the primary diagnostic technique used in this investigation as it is a well established technique for the measurement of plasma properties.

The first portion of this paper provides a discussion of the theory and operation of Langmuir probes for measuring plasma properties, along with the factors which govern interpretation of the probe characteristics. Details of the experimental hardware, data acquisition system, and test facilities are also provided. The major portion of this paper presents a body of experimental data on the plasma properties of the low power arcjet plume. Plasma number density and electron temperature are given as functions of arc power, propellant mass flow rate, mixture ratio, and constrictor geometry. A complete description of the plasma number density distribution is presented for a single operating condition. Measured values of the local flow angle with radial position are also discussed. Finally, a comparison of experimental and theoretical Langmuir probe characteristics and a study of the effective collection area of a spherical probe are given in the appendices.

## NOMENCLATURE

$A_{eff}$	effective probe surface area, $m^2$
$A_e$	nozzle exit area, $m^2$
$A_p$	probe surface area, $m^2$
$A^*$	nozzle throat area, $m^2$
$D_c$	constrictor diameter, m
$D_e$	nozzle exit diameter, m
$D_p$	probe diameter, m
$e$	electron charge, C
$G$	arc gap setting, m
$I$	current, A
$I_{oe}$	electron saturation current, A
$k$	Boltzmann constant, J/K
$L_c$	constrictor length, m
$l$	cylindrical probe length, m
$m$	charged specie mass, kg
$\dot{m}$	mass flow rate, kg/s
$n$	number density, particles/ $m^3$
$Q$	Maxwellian averaged cross section, $cm^3/sec$
$r$	radial distance from center point of nozzle exit plane, m
$R$	radius, m
$S$	ion speed ratio $\frac{U_o}{\sqrt{2kT_e/m_i}}$
$T$	temperature, K

$U_0$	Mean drift velocity, m/s
$V$	voltage or potential, v
$z$	axial distance from thruster exit plane, m
$\chi$	dimensionless potential (Eq. ( A1 ) )
$\lambda$	mean free path, m
$\lambda_D$	Debye length, m

#### Sub- or Superscripts

A	probe designation for fully conducting probe
B	probe designation for conducting/non-conducting sphere
C	probe designation for nonconducting/conducting sphere
act	actual
e	electron
eff	effective
i	ion
max	maximum
min	minimum
n	neutral particles
p	probe
$\infty$	undisturbed plasma

## ANALYSES

### Langmuir Probe Theory and Operation

The Langmuir probe is a widely used technique for the measurement of plasma properties. Briefly, it is a conductive element of known geometry which is connected to a power supply capable of biasing the probe to voltages both positive and negative with respect to the potential of the plasma to be investigated. The current drawn to the probe as a function of applied voltage yields fundamental information on the plasma properties, primarily electron number density and temperature. Excellent reviews of general probe theory and application in both the presence and absence of collisions may be found in Refs. 5 - 8. Laframboise<sup>9</sup> established the theory for both cylindrical and spherical probes in a collisionless, stationary plasma. The application of the Langmuir probe to flowing plasmas ( both collisionless and collisional ) has been investigated by French<sup>10</sup>, Sonin<sup>11</sup>, Clayden<sup>12</sup>, and Graf<sup>13</sup>.

Provided that the probe does not disturb the plasma ( or the macroscopic flow field ) and that the electrons exhibit a Maxwellian distribution, interpretation of the characteristic is reasonably straightforward. In the transition region, the electron current collected by the probe will be given by<sup>11</sup>

$$I_e = A_p e n_e \sqrt{\frac{kT_e}{2\pi m_e}} \exp \left[ \frac{-e(V_p - V_\infty)}{kT_e} \right] \quad (1)$$

Taking the logarithm of Eq. ( 1 ) and differentiating with respect to the probe voltage gives

$$\frac{d}{dV} \ln ( I_e ) = - \frac{e}{kT_e} \quad (2)$$

Consequently, the slope of a semi-log plot of electron current as a function of probe voltage yields electron temperature. Plasma potential is generally located by extrapolating the linear portions of the transition and electron accelerating regions and finding the intersection. Using a thin sheath analysis, the saturation electron current ( at plasma potential ) is given by

$$I_{oe} = A_p e n_e \sqrt{\frac{kT_e}{2\pi m_e}} \quad (3)$$

Rearranging Eq. ( 3 ) yields electron number density in terms of known quantities, as,

$$n_e = (3.73 \times 10^{13}) \frac{I_{oe}}{A_p} \sqrt{\frac{11605}{T_e}} \quad (4)$$

The above analysis is predicated on the assumption that the probe radius is small in comparison with the collision mean free paths but large in comparison with the Debye length; i.e.,

$$\lambda \gg R_p \gg \lambda_D \quad (5)$$

where the Debye length is

$$\lambda_D = 6.93 \times 10^3 \sqrt{\frac{T_e}{n_e}} \quad (6)$$

and  $\lambda$  represents the collision mean paths. As long as the dimensions of the probe are small in comparison with the relevant mean free paths, the theory of Laframboise is a generally accepted means of determining the absolute currents collected by both spherical and cylindrical probes as functions of probe bias voltage,  $R_p/\lambda_D$ , and  $T_i/T_e$ . A method for predicting an ideal V-I characteristic in the collisionless regime is described in Appendix A along with a comparison of an experimental characteristic with an ideal calculation.

#### Effects of Mass Motion

In most plasma flows of interest, the electron random speed is much larger than the directed flow velocity. Previous investigators<sup>10,11,13</sup> have found that cylindrical probes aligned with the flow streamlines behave as though they are in a stationary plasma. Spherical probes are promising because they do not have an alignment constraint; however, even when in free molecule flow with the neutral particles, spherical probe characteristics are influenced by the mass motion. The interaction is similar to that of an orbiting body in a rarefied ionized gas,<sup>14</sup> and is dependent upon potential,  $T_i/T_e$ , and  $R_p/\lambda_D$  as well as ion speed ratio. Clayden<sup>12</sup> has obtained reasonable results using spherical probes in a low density plasma

jet; however, a "wetted" current collection area ( one-half of the spherical surface area ) was used in the calculation of  $n_e$  ( Eq. ( 4 ) ). This modification was made to account for the existence of a wake behind the probe which electrons were unable to penetrate, even though the probe was in near free molecule flow. A previous investigation of the arcjet exhaust using Langmuir probes<sup>4</sup> showed that there was some question of the true collection area of a spherical surface under varied flow conditions. Consequently, as will be described in Appendix B, a portion of the present effort was devoted to determining the effective collection area of spherical probes as a function of the ratio of probe radius to Debye length and the probe potential.

### Effects of Collisions

Collisions between particles in a plasma influence the amount of current collected by a probe. In a flow field where the ionization fraction is small, collisions between charged and neutral species become important. For ion collection, the ion-ion and ion-neutral mean free paths are most important. Similarly, the mean free paths for electron-electron and electron-neutral collisions are relevant for electron collection. For the low density flows of interest here, it is not possible to maintain strict adherence to the above probe sizing criterion ( Eq. ( 5 ) ), particularly with regard to the ion mean free paths. Although the probes used in this investigation remained in free molecule flow with respect to neutral particles, they were not always small with respect to the charged species mean free paths. Table I lists the major collision mean free paths for the range of specie temperatures and densities encountered in this investigation.

Waymouth<sup>15</sup> has presented a theory for the operation of electrostatic probes under thin sheath conditions in plasmas in which the mean free paths are comparable with or smaller than the probe radius ( i.e.,  $R_p/\lambda_D > 100$ ,  $\lambda/R_p < 10$ , and  $\lambda/\lambda_D > 10$  ). He found that the shape of the characteristic near plasma potential becomes distorted due to the probe perturbation of the plasma. The collisions reduce the current at the knee and at positive potentials and the reduction is sensitive to the ratio of  $T_i/T_e$ . For thin sheaths, collisions in the sheath are negligible. The experimental data of French<sup>10</sup>, Sonin<sup>11</sup>, and Graf<sup>13</sup> tend to support Waymouth's conclusions. However, all of the experimental data indicate that, as long as the probe is small compared to the electron mean free paths and that the flow speed is small compared to the electron thermal speed, the electron temperature may be found by the conventional means with a probe of any geometry, independent of its orientation. Further, French<sup>10</sup> has demonstrated that, under the conditions of both mass motion and small ion mean free path, the electron current may still be used to determine  $n_e$ , as long as the mean free paths are much larger than the Debye length.

## EXPERIMENTAL APPARATUS AND PROCEDURE

### Arcjet Thruster Configurations

Figure 1 displays a cross sectional schematic of the low power arcjet anode/nozzle configuration. The thruster discharge region incorporates a vortex stabilized, conventional constricted arc design. The tungsten insert shown in the figure serves both as anode and expansion nozzle. A complete description of the design features of the low power arcjet may be found in Ref. 1. The two laboratory arcjets used in this investigation had internal engine configurations similar to that of the flight-type design but different constrictor dimensions. Table II lists the major components and dimensions of interest for the two arcjets. The component materials for the two thrusters were identical except for the anode housings. For Thruster A ( 0.038 cm  $D_c$  ), the housing was fabricated from titanium zirconium molybdenum while, for Thruster B ( 0.064 cm  $D_c$  ), it was made from stainless steel. The different material selection enabled a larger operating range for the molybdenum thruster. Both of the anode inserts were fabricated from two-percent thoriated tungsten with a converging half angle of 30° and a diverging half angle of 20°. The arc gap setting for both thrusters was 0.058 cm. No attempt was made to vary this parameter for the present investigation. The area ratio of Thruster A was 600 while that of Thruster B was 220.

Typical operating conditions and performance characteristics for the two arcjet thrusters may be found in Table III. Recent experiments<sup>16</sup> have documented the relative effects of nozzle configuration on arcjet

operating characteristics. It was concluded that the contour of the divergent section of the nozzle/anode had a significant impact on arcjet performance, as it determined the location of arc attachment. A conical nozzle exhibited optimal performance. Since the anodes used in this investigation had the same divergent contour, the slight differences in measured performance were primarily due to plasma/gas dynamics in the constrictor region as it is not expected that arc attachment for the two configurations varied significantly. In general, Thruster B ( larger  $D_c$  ) produced a higher thrust than Thruster A for the same ratio of arc power to mass flow rate although the overall efficiency and specific impulse were slightly lower.

The arcjets operated on mixtures of nitrogen and hydrogen to simulate fully decomposed hydrazine and ammonia. A 3:5:2 mixture of nitrogen, hydrogen, and ammonia was also used to simulate the gas mixture exiting a hydrazine catalyst bed. Typical mass flow rates ranged from 22 - 38 mg/s for Thruster A and 33 - 45 mg/sec for Thruster B. The latter thruster was also operated with pure ammonia at 52-58 mg/sec. The gases were stored separately and mixed upstream of the thruster inlet. Digital flow meters, calibrated for the specific gas type, were used in conjunction with a flow controller to set and monitor individual volume flow rates. Arc power was provided from a well-regulated ( 10 percent ripple ), pulse width modulated supply.<sup>17</sup> The arc current was measured using a Hall effect current probe while arc voltage was measured with a high impedance divider network. The entire system operated with the arcjet anode tied to facility ground. Typical values of arc current ranged from 6 - 12 A, depending on the thruster configuration and mass flow rate.

### Langmuir Probes

Langmuir probes of both spherical and cylindrical geometry were used in this investigation. The spherical probes were made of carbide steel bearing balls with radii of 0.951 and 0.554 cm. Each ball was silver soldered to a 0.76 mm tungsten wire. Stainless steel tubing was used to support the probe and alumina served as the insulator between the tube and probe. The cylindrical Langmuir probe was made of tungsten wire of radius 0.075 cm and length 2.38 cm and had the same type of support as the spherical probes. Further details of the design and construction of the Langmuir probes may be found in Ref. 4.

Figure 2 displays an electrical schematic of the probe bias circuitry. The bias supply linearly ramped the probe voltage from a preselected negative value ( - 3 v ) to a positive value ( + 3 v ) over a 2.2 sec time period. The probe measurements were referenced to the arcjet anode which was connected to facility ground. The probe voltage was measured directly across the output of the power supply while the probe current was obtained by measuring the voltage across a 101  $\Omega$  resistor. Since the voltage drop across the resistor was not negligible, a correction was applied to the measured voltage during data reduction to obtain the actual probe voltage. The current and voltage signals were recorded by a digital storage oscilloscope and then sent to a personal computer for subsequent data reduction and storage. The above data acquisition process permitted a large number of complete probe characteristics to be taken during a given test period for later analysis. The estimated uncertainty in the probe current measurement was 50 - 100  $\mu$ A.

### Test Facility and Experimental Set-up

The majority of the arcjet plume surveys were conducted in a 4.4 m diameter x 19 m long vacuum facility ( Tank 5 ). The vacuum tank was equipped with twenty, 32-in diameter oil diffusion pumps backed by four rotary blowers and four mechanical roughing pumps. It maintained background pressures less than  $2.6 \times 10^{-2}$  Pa (  $2.0 \times 10^{-4}$  Torr ) throughout the experiments.

A photograph of the experimental apparatus and set-up is displayed in Figure 3. As shown, three Langmuir probes were mounted on an actuator system capable of linear motion in directions both parallel to and perpendicular to the thrust axis. The radial traversing mechanism covered distances of approximately  $\pm 0.5$  m off the plume centerline while axial motion ranged from within 12 cm of the thruster exit plane to 1.1 m downstream. The cylindrical Langmuir probe ( center probe in the figure ) was mounted on a rotary actuator such that it could rotate about a single point of reference for the purpose of studying local flow angle variation. The two spherical probes were mounted on either side and remained fixed with respect to the center probe's rotary motion.

## Procedure

The arcjet thruster was mounted on a linear actuator which positioned the thruster inside the tank, as shown in Fig. 3. The probes were fixed at their predetermined locations prior to the experiment and the relative positions of the probes with respect to the center of the arcjet nozzle exit were calibrated every time the vacuum tank was opened. A low power laser was used in conjunction with the center probe to ensure that the probe remained in the same vertical plane throughout its axial traverse. Axial and radial calibration of the actuators was accomplished with discrete measurements of the probe location, creating a linear plot of the actual versus indicated distance. Rotary motion of the center probe was calibrated in a similar fashion. The estimated uncertainty in an individual probe's position was  $\pm 0.2$  cm which is less than twenty percent of the spherical probe dimensions.

The Langmuir probes were cleaned chemically before placement in the tank and every time the tank was cycled. It was not possible to heat the large probes sufficiently with a positive bias to get the temperature high enough for emissive cleaning. At least 2200 K for a few sec is needed to remove a monolayer of  $N_2$  deposited on the surface of the probe.<sup>13</sup> An ohmmeter was used to verify probe surface conductivity every time the tank was cycled. However, the effect of a changing and/or variable work function on a probe characteristic due to the presence of adsorbed  $N_2$  on the probe surface will be discussed in a subsequent section of this report.

Generally, the thruster was allowed to run for at least 30 min after the arc discharge was initiated so that it could reach a thermally stable condition. Subsequent changes to thruster operation, such as variations in arc current, required only a few minutes for the arcjet to reach a new steady state operating condition. The arc current, arc voltage, propellant mass flow rates, and tank pressure were recorded periodically during the experiments. Previous measurements<sup>4</sup> 30 cm downstream of the thruster indicated that, at a constant mass flow rate,  $n_e$  increased significantly with arc power. For the present experiments, data were taken over a greater range of arc power and mass flow rates for mixture ratios of both 1:2 and 1:3 of  $N_2:H_2$ . An axial distance of 30 cm was again chosen as the location for the measurements since the density levels at that location are sufficiently high to impact the transmission of RF communications signals.<sup>3</sup>

Positional surveys were also taken at various locations in the plumes of Thrusters A and B. Radial surveys on both sides of the thrust centerline were taken at axial distances of 12.1 cm, 18.8 cm, 32.0 cm, and 64.5 cm. Axial surveys were taken along the thrust centerline and at the outermost radial location ( 57.6 cm ).

The current-voltage characteristic of a Langmuir probe was recorded by a digital storage oscilloscope and then transferred to a computer for storage and subsequent analysis. Approximately 2000 data pairs of voltage and total probe current were obtained for each probe sweep. Since the probe voltage was swept slowly, the total current collected by the probe reflected the temporal behavior of the plasma due to the AC ripple of the power supply; consequently, the total current data had to be smoothed with two, 16 point averaging routines. The fluctuations were generally less than 0.2 mA and were insignificant in the electron saturation portion of a V-I characteristic; however, they were the predominant cause of measurement uncertainty in the determination of electron temperature. Also, because the voltage was measured at the output of the power supply, the actual probe voltage was calculated by subtracting the smoothed current times the measurement resistance. The ion contribution was then subtracted from the total current to obtain the final set of probe voltage and electron current pairs. Least-squares fits were used to extrapolate the linear portions of the transition and electron accelerating regions of the characteristic. Plasma potential and the electron saturation current were defined at the point of intersection. The electron temperature was determined from the reciprocal of the slope of the line through the transition region and Eq ( 4 ) was used to determine  $n_e$ . For the cylindrical probe data, the total surface area of the probe was used in Eq ( 4 ); however, for the spherical probe data, an effective collection area of 70 percent was used as will be discussed in Appendix B.

In a flowing plasma, the magnitude of the saturation current depends upon the relative orientation of the flow and the cylindrical probe. If the ratio of  $R_p/\lambda_D \gg 1$  and the flow is supersonic, the ion saturation



current reaches a minimum when the probe is aligned with the flow streamline.<sup>18</sup> A similar result is predicted for  $R_p/\lambda_D \ll 1$ , as long as probe end effects are negligible.<sup>7</sup> The dependence on probe orientation was utilized to measure the local velocity vector as a function of position in the exhaust. The probe was biased to + 3 V and the electron current to the cylindrical probe was recorded as a function of rotary angle with respect to the plume centerline. As will be shown in a subsequent section, the positive probe bias produced a minimum in probe current at the angle of the flow streamline. Data were taken on both sides of centerline at axial distances of 12.2, 16.0, and 18.5 cm.

## RESULTS AND DISCUSSION

This section summarizes the results of the Langmuir probe surveys in the exhaust of a low power, dc arcjet thruster. The plasma plumes of the two different constrictor/nozzle geometries are described at a location 32 cm downstream of the exit as a function of arc power, propellant mass flow rate, and mixture ratio. Positional variations in electron number density and the local flow angle are also illustrated. A comparison of an experimental V-I characteristic of a spherical Langmuir probe with an ideal calculation is presented in Appendix A. Appendix B presents preliminary results in the study of the effective collection area of a spherical probe as a function of the ratio of probe radius to Debye length and the probe potential.

### Variations in Plasma Properties with Arcjet Operating Condition and Constrictor Geometry

Figures 4 and 5 present cumulative plasma number density and electron temperature data for the two thruster configurations at a location on the plume centerline, approximately 32 cm downstream of the exit. The two thrusters operated on mixtures of  $N_2$ ,  $H_2$ , and  $NH_3$  to simulate the decomposition products of hydrazine and ammonia. The different symbols in the plots denote combined variations in mixture ratio and mass flow rate. Since the trends for the two thruster configurations are similar, they will be addressed together. Because a set arc current did not always give the a consistent arc voltage, the measured electron number density values are plotted as a function of arc power. The calculated uncertainties in the 1:2 and 1:3 mixture ratio data mostly vary from 10 - 50 %, primarily due to the large uncertainties in relatively low values of measured electron temperatures. The data for pure ammonia with Thruster B varied in calculated uncertainties from 25 - 60%. However, within the limitations of the measurement technique, there is a reasonable consistency in the measured data. As demonstrated in a preliminary investigation,<sup>4</sup> the measured electron number density increases dramatically with arc power at a constant mass flow rate. For Thruster B ( Fig. 4 ( a ) ), the increase in  $n_e$  with arc power appears smaller than for Thruster A ( Fig. 5 ( a ) ) although Thruster B had a much smaller operating envelope. There appears to be some noticeable scatter in the measured  $n_e$  for Thruster A, particularly for the 1:2 mixture ratio at 34 mg/s; however, many of these data points were taken during the first day of testing when arc voltage fluctuations tended to be most severe. In general, a fifty percent increase in arc power results in a factor of 2-3 increase in the measured electron number density. For both 1:2 and 1:3 mixture ratios, there is only a slight increase in number density with increasing mass flow rate for a given arc power. The 1:3 mixture also produced higher values of  $n_e$  than did the 1:2 mixtures, presumably due to the presence of more hydrogen. Finally, it is interesting to note that thruster operation with simulated, fully decomposed ammonia ( 1:3 mix ) resulted in much higher values of centerline electron number density than did the pure ammonia operation.

Figures 4 ( b ) and 5 ( b ) display the corresponding values of measured electron temperature for Thrusters B and A, respectively. As in the preliminary investigation<sup>4</sup>, a systematic variation in electron temperature with arc current, arc voltage, or arc power is not evident, as the scatter in the data is fairly large. For the two thrusters tested in this investigation, the measured electron temperatures appear to be more consistent ( 0.1 - 0.2 eV ) but much lower than those of the arcjet tested previously ( 0.4 - 0.8 eV ). It is apparent from the variations in  $n_e$  and  $kT_e$  with arc power and mass flow rate, that individual thrusters have distinct plume characters; however, the limited amount of data taken to date are insufficient to separate the roles that such variables as arc gap setting, arc anode attachment, constrictor/nozzle geometry, mixture ratio and strength of vortex propellant flow have on the charged species distribution in the exhaust. However, it is important to document the trends which do exist and establish a body of experimental data for subsequent analysis when the gas/plasma dynamics of the internal arcjet are better understood.

In general, the plasma plumes of the two arcjet thrusters exhibited the same experimental trends; that is, as long as the arcjet maintained a constant arc voltage for a given arc current, an increase in centerline electron number density was observed with increasing arc power at a constant mass flow rate or with increasing mass flow rate at a constant current. These trends are also evident in the data of Figure 6 ( a ), which plots the measured electron number density as a function of specific power ( the ratio of arc power to mass flow rate ) for Thruster A. Some of the data taken during the first test date with this thruster have been excluded from the plot. As seen in the figure, an increase in specific power results in an increase in the measured electron number density at a constant mass flow rate; however, increasing the specific power at constant current ( e.g., corresponding to a decrease in mass flow rate ) results in a decrease in  $n_e$ . It is expected that the observed trends in measured plasma number density in the plume should be consistent with arcjet performance characteristics. Because the electron number density profile does not vary significantly with thruster operating conditions, the measured centerline electron number density is indicative of the relative amount of frozen flow losses. Figure 6 ( b ) plots the overall efficiency as a function of specific power for Thruster A operating on a 1:2 mixture ratio of  $N_2:H_2$  at two different mass flow rates. The observed decrease in overall efficiency with increasing arc current at a constant mass flow rate is qualitatively consistent with the plume electron number density trends. The trends for decreasing mass flow rate at constant current, however, are in direct contrast. It would seem that, at a higher mass flow rate, recombination would be enhanced by the higher pressure and the frozen flow losses would decrease. The performance characterization reflects that this may indeed be the case in that overall thruster efficiency does improve with mass flow rate at constant specific power. However, the electron number density increases under these same conditions ( Fig. 6 ( a ) ). One possible explanation<sup>19</sup> may be that, at higher mass flow rates, the arc becomes more constricted; consequently, the value of centerline enthalpy may be higher resulting a higher centerline plasma number density. Further quantitative data near the exit of the arcjet nozzle are needed to fully the observed plasma plume anomalies.

#### Plasma Number Density Distribution in the Arcjet Plume

The spherical probes were used to obtain radial profiles at axial distances of 12.1, 18.8, 32.0, and 64.5 cm downstream of the thruster exit plane. A centerline data point was also taken with the cylindrical probe at  $z = 12.1$  cm. Axial surveys were also taken along the thrust centerline and at a radial distance of 57.6 cm. Figure 7 displays a 3-dimensional plot of the measured electron number density distribution of Thruster B operating on a 1:2 mixture ratio of  $N_2:H_2$  at a mass flow rate of 43.4 mg/s. The arc current was 10.2 A. Based on the measurements, the Debye lengths were on the order of  $10^{-3}$  to  $10^{-2}$  cm so the ion density distribution should display a similar profile to maintain plasma neutrality. In a medium where the ionization fraction is very low ( much less than one percent ), as in the case of the arcjet exhaust, the ion-electron mean free paths are considerably larger than for charged specie-neutral collisions. Therefore, it is not expected that ambipolar diffusion rates determine the charged specie distribution in the plume. Rather, they are a direct consequence of the gas dynamic expansion of neutral species. The ions will tend to follow the neutral gas distribution due to high ion-neutral collision rates and hold the faster moving electrons back.

Radial profiles were also taken with the thrusters operating on different mixture ratios, arc currents, and flow rates. Although not detailed in this report, the trends repeat the findings of the preliminary investigation.<sup>4</sup> There is an exponential decrease in measured number density as a function of angle off centerline and an inverse distance-squared decrease in number density along centerline.

#### Flow Angle Determinations Using Cylindrical Langmuir Probes

The response of cylindrical Langmuir probes is extremely sensitive to the relative probe orientation with the flow streamlines. This dependence on probe orientation was utilized to measure the local velocity vector as a function of position in the exhaust. The probe was biased to + 3 V and the electron current to the cylindrical probe was recorded as a function of rotary angle with respect to the thrust centerline. Figure 8 ( a ) displays the measured electron current to the probe as a function of probe angle with respect to the plume centerline for the cylindrical Langmuir probe located on the thrust centerline, 18.5 cm downstream of the exit. The solid data points are from a survey taken 25 min later in time than the open symbol points. The minimum at  $0^\circ$  with respect to the thrust centerline denotes the local flow angle of  $0^\circ$ , as expected.

Values of local flow angle based on the cylindrical probe measurements are plotted in Figure 8 ( b ) as a function of radial distance from centerline at axial distances of 12.2, 16.0, and 18.5 cm. The increase in flow angle with axial distance reflects the particle expansion. The same data are plotted in Figure 8 ( c ) as a function of angle off centerline. The solid line in the figure denotes radial flow. The fact that the measured flow angle and the geometric angle off the nozzle axis agree indicates that the flow is source-like in nature at dimensionless distances of  $z/D_e > 10$ .

## CONCLUDING REMARKS

Langmuir probes of cylindrical and spherical geometry have been used to investigate the plumes of low power, dc arcjet thrusters operating on mixtures of nitrogen, hydrogen, and ammonia to simulate the decomposition products of hydrazine and ammonia. This paper extended previous work and presented a body of experimental data which correlate measured plasma properties in the arcjet plume with thruster operating conditions for two different constrictor/nozzle geometries. It is apparent from the variations in  $n_e$  and  $kT_e$  with arc power, mass flow rate, and mixture ratio that arcjet thruster plumes can be quite sensitive to design and operating condition. The data taken to date, however, are insufficient to determine the relative effects of such variables as arc gap setting, arc anode attachment, constrictor/nozzle geometry and strength of vortex propellant flow on the charged species distribution in the exhaust. The trends which do exist have been documented for subsequent analyses when the gas/plasma dynamics of the internal arcjet are better understood.

In general, the plasma plumes of the two arcjet thruster configurations exhibited the same experimental trends; that is, as long as the arcjet maintained a nonfluctuating voltage for a given arc current, an increase in centerline electron number density was observed with increasing arc power at a constant mass flow rate or with increasing mass flow rate at a constant current. A 1:3 mixture of  $N_2:H_2$  produced higher values of  $n_e$  than did 1:2 mixtures, presumably due to the presence of more hydrogen. Also, thruster operation with the 1:3 mixture of  $N_2:H_2$  resulted in much higher values of centerline electron number density than did pure ammonia operation. Typically, the trends appeared to be more pronounced for the thruster with a smaller constrictor diameter. The measured electron temperatures consistently ranged between 0.1 - 0.2 eV for both thrusters but no systematic variation with arc current, arc voltage, or mass flow rate was observed.

The measured electron number density decreases exponentially as a function of angle off centerline and as the inverse distance-squared along centerline. Radial profiles taken with the thrusters under different operating conditions produced similar trends. Finally, the use of a cylindrical probe for the determination of local flow angle was demonstrated. At dimensionless distances  $z/D_e > 10$ , the measured local flow angle was equal to that of the geometric angle with respect to centerline, indicating that the flow was source-like in nature.

It is apparent that more work is needed to fully document the arcjet plume, particularly close to the nozzle exit. Spherical probes are promising because they do not have an alignment constraint but more work is needed to understand the presence of wake effects and the correct application of an effective probe area. Significant progress in the field of Langmuir probes has been made in understanding the idealized current collected by both cylindrical and spherical probes. Unfortunately, the theories are all based on an idealized, a priori knowledge of the major plasma parameters. It is much more difficult to extract information of the plasma properties ( such as ion temperature or ion mass) from an experimental V-I characteristic. A combination of intrusive probe and non-intrusive diagnostic techniques are required to unambiguously obtain this information on the arcjet plasma plume.

## APPENDIX A - Collisionless Theories for Electron and Ion Current Collection

### Theory and Development of Equations for Ideal Probe Characteristics

In a collisionless plasma, the theory of Laframboise for both spherical and cylindrical probes was developed for a Maxwellian plasma at rest for the regime defined by

$$\begin{aligned} 0 &\leq T_i/T_e \leq 1 \\ 0 &\leq R_p/\lambda_D \leq 100 \\ \text{and} \quad |\chi_p| &\leq 25 \end{aligned}$$

where  $\chi_p$  is the dimensionless probe potential given by

$$\chi_p = e(V_p - V_\infty) / k T_e \quad (A1)$$

The calculations of Laframboise assume that the dominant influence on the motion of the charged particles is the electric field consistent with Poisson's equation. For a two temperature plasma consisting of two species of charged particles (electrons and singly charged ions), the Vaslov equations governing the particle dynamics for the two species are coupled by Poisson's equation and solved iteratively. The absolute magnitudes of the ion and electron current densities collected by the probe as a function of probe potential may be summarized by the following relationships:<sup>11</sup>

For  $\chi_p < 0$ ,

$$j_i = e n_\infty \sqrt{\frac{k T_e}{2\pi m_i}} I_i^* (\chi_p R_p / \lambda_D T_i / T_e) \quad (A2)$$

$$j_e = e n_\infty \sqrt{\frac{k T_e}{2\pi m_e}} e^{\chi_p} \quad (A3)$$

For  $\chi_p > 0$ ,

$$j_i = e n_\infty \sqrt{\frac{k T_i}{2\pi m_i}} e^{-\left[\frac{T_e}{T_i}\right] \chi_p} \quad (A4)$$

$$j_e = e n_\infty \sqrt{\frac{k T_e}{2\pi m_e}} I_e^* (\chi_p R_p / \lambda_D T_i / T_e) \quad (A5)$$

For  $\chi_p < -10$ , only ions are collected by a probe. For  $\chi_p > -10$ , both ions and electrons are collected by the probe. However, a widely used means of extracting the electron current from this portion of the characteristic is to extrapolate the ion current curve from  $\chi_p < -10$  to higher potentials.<sup>6</sup> In a plasma where the distribution of electrons is Maxwellian, the electron current collection in the transition region will

increase exponentially. For  $\chi_p > -1$ , the ion current collection becomes negligible until only electrons are collected.

$I_i^*$  and  $I_e^*$  in the above equations are dimensionless ion and electron currents, respectively, and are of order unity for moderate potentials. Kiel<sup>20,21</sup> and Peterson-Talbot<sup>22</sup> have presented simplified methods for the calculation of  $I_i^*$  and  $I_e^*$  as functions of dimensionless potential,  $R_p/\lambda_D$ , and  $T_i/T_e$ . In particular, Kiel<sup>20</sup> developed an analytical expression for the saturation current regimes of a free-molecular spherical probe with a finite sheath. The expression is valid for  $T_i/T_e > 0.01$  and probe potentials large compared to the floating potential. Debye lengths must be sufficiently small to ensure formation of a sheath ( $R_p/\lambda_D > 3$ ).

The current drawn to the probe as a function of voltage is dependent upon parameters involving the sheath thickness and the electrostatic potential at the edge of the sheath. To determine the sheath thickness, Kiel derived an empirical expression to fit the more exact numerical solutions of the potential fields. The electrostatic potential was obtained from a transcendental equation and depended only on the ratio of  $T_i/T_e$ . For large probe potentials, Kiel's expression agreed reasonably well with the numerical solution of Laframboise. Complete details of Kiel's technique and the derivation of equations may be found in Refs. 20 and 21. The method of Kiel was used to generate ideal characteristics for comparison with experimental data. Since the calculated Kiel values of  $I_i^*$  and  $I_e^*$  approach unity for small probe potentials (i.e., as  $V_p$  approaches  $V_\infty$ ), this method was used beyond the stated range of validity so a complete characteristic could be obtained for purposes of comparison.

#### Comparison of an Experimental V-I Characteristic with an Ideal Calculation

Figure 9 displays a comparison of measured and calculated Langmuir spherical probe response in terms of current collection as a function of probe voltage. The measurement was taken with the spherical probe ( $R_p = 0.554$  cm) at a radial location 35.3 cm off centerline and 18.8 cm downstream of the thruster exit. The calculated values are based on ratios of  $T_i/T_e$  of 0.01 and 1.0. On a logarithmic plot (Fig. 9 (a)), the agreement between experiment and theory is excellent. The linear variation of electron current over at least two orders of magnitude is indicative of a Maxwellian distribution of electron velocities. The measured electron temperature based on the inverse of the slope of a least squares fit through the transition region is  $1578 \text{ K} \pm 580 \text{ K}$ . The measured electron number density is  $5.5 \times 10^8/\text{cm}^3$  with a measurement uncertainty of 28%. No correction was made to the probe area as  $R_p/\lambda_D$  for this case was only 47. When plotted on a linear scale (Fig. 9 (b)), the data more clearly show a marked difference between experiment and theory in the functional dependency of electron current with probe voltage. Here the measured electron current is compared against calculated values for  $T_i/T_e = 0.01, 0.1$ , and  $0.2$ . The deviation is due in part to the breakdown of Kiel's theory for values of dimensionless potential  $\chi_p \leq 3$ . However, there is also a good reason to suspect that variations in work function of the probe surface contributed to the discrepancy. Firstly, the probe voltage was swept slowly enough (2.2 sec) that thermal variations in the probe surface could occur, and secondly, the presence of  $N_2$  monolayers on the probe surface may have altered the surface work function. For this particular characteristic, the sheath was thin, and the relevant collision mean free paths were all larger than the probe radius. It is therefore unlikely that collisions played a role in the variation of the measured  $I_e$  curve from the ideal. Finally, since electron current collection in the saturation region is independent of ion mass, it seems reasonable to assume that the ion temperature at this location is much less than the measured electron temperature ( $T_i < 0.2 T_e$ ).

Figure 9 (c) presents a comparison of experimental and ideal calculated values of current collected by the spherical probe at negative potentials. Total probe current is plotted rather than ion current although the electron current may be assumed to be negligible for values of dimensionless potential  $\chi_p$  less than -10. For the ideal calculation, the description of ion current collection in this region is highly dependent on an accurate knowledge of the ratio of ion temperature to electron temperature and the ion mass. Since these two parameters are not known with absolute certainty, the ideal curves were generated for two different temperature ratios ( $T_i/T_e$  of 0.1 and 0.2) and ion masses ( $3 \times 10^{-27}$  and  $4 \times 10^{-27}$  kg). It should be

mentioned that these values of ion mass are considerably lower than that which would be calculated from an average molecular weight of the gas mixture ( assuming the ion mass is equal to the average neutral mass of  $1.77 \times 10^{-26}$  kg ). Using the higher ion mass resulted in electron currents which are much too small. The fact that the lower values were needed to give good agreement between theory and experiment may indicate that the ionized species in the plume are mostly atomic hydrogen ions; however, given the fact that the collected ion currents are on the same order as the measurement uncertainty, no definitive conclusions can be drawn at this time. Spectroscopic data are needed to determine relative specie populations in the arcjet plume.

## APPENDIX B - Study of Probe Effective Collection Area

### Experimental Apparatus and Procedure

Because of the uncertainty in the true collection area of a spherical probe in a flowing plasma, a portion of the present effort was devoted to the determination of the true collection area of a spherical probe in a flowing plasma. Three probes of equivalent spherical geometry but varied composition were constructed. The diameter of each probe was 1.91 cm ( 0.750 in ). The first probe, designated as Probe A, was fabricated from a solid carbide steel bearing ball. Probes B and C were constructed of a solid carbide steel hemisphere bonded to a ceramic hemisphere with a high temperature ceramic adhesive. The conducting half of probe B and the nonconducting half of Probe C faced toward the arcjet thruster exit. The individual probe characteristics could be uniquely determined using the same data acquisition system previously described. Additionally, the probe voltage could be varied manually with measurement of the actual probe voltage displayed on a digital multimeter. The current collected by the probe was also measured across a 101 ohm resistance by a digital multimeter.

The experiments were conducted in a 1.5 m diameter by 5 m long vacuum chamber ( Tank 8 ) equipped with four, 0.82 m diameter oil diffusion pumps. The background pressure during the experiment was maintained below  $6.7 \times 10^{-2}$  Pa (  $5 \times 10^{-4}$  Torr ). Figure 10 presents a photograph of the experimental set-up for the effective probe area studies. As shown, the three probes were mounted 17.8 cm on a single rake, which was attached to a linear actuator capable of motion across the jet ( i.e., perpendicular to the thrust centerline). The arcjet thruster was mounted on a cradle connected to a push-pull rod that extended the arcjet into the vacuum tank. Once in place, it rested on a fixed table to ensure that the thruster position was stable and repeatable from one test date to the next. The push-pull rod was also used to vary the axial distance between the thruster exit plane and the probes. With this configuration, axial distances were limited to a range from 7.6 cm to 38.9 cm. Placement accuracy was  $\pm 0.3$  cm. The radial positions of the probes in the flow field were given by a calibrated potentiometer mounted on the actuator assembly. The linear actuator allowed repeatable positioning of the probes on centerline to an accuracy greater than 0.02 cm over a 35.6 cm range of motion. However, during actual operation of the vacuum facility, the probe positioning accuracy was significantly impacted by the presence of tank vibrations which resulted in a oscillatory probe motion. The positioning accuracy during the measurements was estimated to be  $\pm 0.5$  cm.

Thruster A was used in this experiment, operating at an arc current of 11 A with a resultant arc voltage of 117 v. The mass flow rate was 34 mg/sec using a 1:2 mixture of  $N_2:H_2$ . Probe data were taken in the following manner for the single thruster operating condition. The fully conducting probe (Probe A ) was positioned on the centerline of the exhaust. The axial position was set and recorded. The voltage across the probe was varied from -5 v to + 5 v in 1 v increments with the total probe current recorded at each voltage. The data were taken at several axial positions ranging from 38.9 cm to 7.6 cm. It was not possible to obtain data at distances greater than 38.9 cm without having the thruster support structures interfere with the plume expansion. Probe B was then placed on centerline and current data for all eleven voltages were taken at the same axial locations as Probe A. Finally, the same procedure was repeated for Probe C. Approximately forty-five minutes elapsed during data acquisition for the three probes. During this time the arc voltage varied less than one percent, so it is not expected that fluctuations in arcjet operating condition significantly affected the probe current collection. Complete V-I characteristics of the three probes were recorded at  $z = 30.5$  cm.

Since the current collected by a Langmuir probe is directly proportional to the true collection area, an effective probe area may be calculated using values of currents collected by the three probes while at the same potential. The two methods which were used to calculate the effective current collecting area of Probe A are given below. In both methods it was assumed that wake effects, if present, would only disturb the back hemisphere; therefore, for a spherical Langmuir probe in which the effective collection area is the actual surface area of the probe (  $4\pi R_p^2$  ), the amount of current collected should be twice that of Probe B. The ratio of the sum of the currents collected by Probes B and C to their total effective collection area should equal the current density of a fully conducting spherical probe. Edge effects between the conducting

and non-conducting portions of Probes B and C were neglected. Method 1 can be expressed by the following equation:

$$\frac{I_B + I_C}{A_{\text{eff}}} = \frac{2I_B}{A_{\text{act}}} \quad (\text{B1})$$

Similarly, the current density of Probe A, based on an effective collection area, should also equal that of a fully conducting probe. Method 2 is given by

$$\frac{I_A}{A_{\text{eff}}} = \frac{2I_B}{A_{\text{act}}} \quad (\text{B2})$$

Equations (B1) and (B2) do not distinguish between ion or electron current, as the total probe current was measured; however, a previous study<sup>4</sup> has indicated that when  $|V_p| \geq 1.0$  v, the probe is operating in a saturation regime (i.e., collecting only ions or electrons).

### Preliminary Results and Discussion

The three complete V-I characteristics of the different probe configurations yielded good agreement in measured number density when the effective probe areas were considered. The measured electron temperatures agreed to within thirty percent (the measurement uncertainty). The electron number density as a function of axial distance was determined from the complete V-I characteristic at  $z = 30.5$  cm and from inferred values based on the electron saturation currents collected by Probe A at the various locations.

The ratio of the effective collection area to the actual probe area was calculated using the methods described by Eqs. (B1) and (B2). The two methods provided reasonably similar results, although Method 2 appears to produce a slightly higher effective area than Method 1. The cause could be attributed in part to the presence of a small amount of ceramic adhesive that contaminated a section a few tenths of a millimeter wide on the conducting hemisphere of Probe C (which was used in the data analysis of Method 1). For  $|V_p| \geq 3$  v, the two calculation techniques agreed to within four percent. For  $|V_p| \leq 2$  v, the differences varied as much as seven percent. It does not seem likely that a distortion of the sheath at the edges of Probes B and C contributed to the discrepancy, since the probes were all operated in a thin sheath mode.

Figure 11 presents the ratio of the effective collection area of the fully conducting probe to its actual surface area as a function of the ratio of probe radius to Debye length for both positive and negative probe bias voltages. The values of the effective collection areas are based on the average values calculated by Methods 1 and 2. For positive bias voltages (Fig. 11 (a)), the effective probe area decreases from 75% at  $R_p/\lambda_D$  of 100 to 55% as  $R_p/\lambda_D$  approaches 600. A similar trend is observed for negative bias voltages, as seen in Fig. 11 (b). For  $R_p/\lambda_D > 200$ , the probe is definitely in continuum flow with respect to the ion motion. For supersonic plasma flows, a shock consisting only of ions and electrons is predicted for these conditions.<sup>10</sup> Even at the closest data point,  $z = 7.6$  cm, the probe was only in transitional flow with respect to the neutral particle motion ( $\lambda/R_p \sim 2$ ). Because of the probe size and the limitations of the positioning apparatus, it was not possible to obtain effective area data for  $R_p/\lambda_D < 100$ . However, the data of a previous study<sup>4</sup> seems to indicate that, for  $R_p/\lambda_D \ll 100$ , it is possible for a spherical probe to have an effective area which approaches the total probe surface area. It should be noted that the Langmuir probes used in the plasma plume surveys in Tank 5, had typical values of  $R_p/\lambda_D$  much less than 200. An effective probe area of 70% was used in all data reduction, as it seemed to be a reasonable average for the range of  $R_p/\lambda_D$  encountered. The positional variation in electron number density decreases almost two orders of magnitude within 50 cm; consequently, a constant effective area for all measurements would not introduce an unacceptable error in the number density profiles, as long as one accepts a measurement uncertainty of at least 30 percent.



## ACKNOWLEDGEMENTS

The authors wish to express appreciation to Mr. Robert S. Jankovsky of the University of Akron for his assistance in conducting the experiments on the probe effective collection area. Also, the following individuals provided valuable technical support in the design, fabrication, and implementation of the Langmuir probe experiments: Messrs. Vincent E. Satterwhite, Charles A. Reuger, Eugene S. Pleban, Carl A. Ollick, and Craig N. Horak.

## REFERENCES

1. Curran, F. M. and Haag, T. W., "An Extended Life and Performance Test of a Low Power Arcjet," AIAA Paper 88-3106, July 1988.
2. Knowles, S. and Yano, S., "Engineering Model Low Power Arcjet System Development," Rocket Research Company, presented at the 1989 JANNAF Propulsion Meeting, Cleveland, Ohio, May, 1989.
3. Carney, L. M., "Evaluation of the Communications Impact of a Low Power Arcjet Thruster," AIAA Paper 88-3105, July, 1988.
4. Carney, L. M., "An Experimental Investigation of an Arcjet Thruster Exhaust Using Langmuir Probes," Master's Thesis, University of Toledo, NASA TM-100258, December, 1988.
5. Chen, F., Electric Probes., Plasma Diagnostic Techniques, R. H. Huddleston and S. L. Leonard, eds., Academic Press, 1965.
6. de Leeuw, J. J., Electrostatic Plasma Probes, Physico-Chemical Diagnostics of Plasma, T.P. Anderson, R.W. Springer, and R.C. Warder, Jr. eds., Northwestern University Press, 1964, pp. 65- 95. ( AIAA Paper 63-370).
7. Chung, P. M., Talbot, L. and Touryan, K. J., Electric Probes in Stationary and Flowing Plasma. Theory and Application, Springer-Verlag, 1975.
8. Swift, J. D. and Schwar, M. J., Electrical Probes for Plasma Diagnostics, London Iliffe Books, 1970.
9. Laframboise, J. G., "Theory and Spherical and Cylindrical Langmuir Probes in a Collisionless, Maxwellian Plasma at Rest," University of Toronto Institute for Aerospace Studies, UTIAS-100, June, 1966. (Avail. NTIS AD-634596).
10. French, J. B., "Langmuir Probes in a Flowing Low Density Plasma," AFOSR-2159, UTIA-79, University of Toronto Institute for Aerophysics, August, 1961.
11. Sonin, A. A., "The Behaviour of Free Molecule Cylindrical Langmuir Probes in Supersonic Flows, and Their Application to the Study of the Blunt Body Stagnation Layer," UTIAS-109, University of Toronto Institute for Aerospace Studies, August, 1965. ( Avail. NTIS AD-626451 ).
12. Clayden, W. A., "Langmuir Probe Measurements in the R.A.R.D.E. Plasma Jet," Third International Symposium on Rarefied Gas Dynamics, Advances in Applied Mechanics, Vol. 2, J.A. Laurmann, ed., Academic Press, 1962, pp. 435-470.
13. Graf, K. A., "The Determination of Spatially Non-Uniform Electron Density Distribution," University of Toronto Institute for Aerospace Studies, UTIAS-108, April, 1965.

14. Stone, N. H., "The Aerodynamics of Bodies in a Rarefied Ionized Gas with Applications to Spacecraft Environmental Dynamics," NASA TP 1933, November, 1981.
15. Waymouth, J. F., "Perturbation of a Plasma by a Probe," *The Physics of Fluids*, Vol. 7, No. 11, November, 1964, pp. 1843-1854.
16. Curran, F. M., Sovie, A. J., and Haag, T. W., "Arcjet Nozzle Design Impacts," presented at the 1989 JANNAF Propulsion Meeting, Cleveland, OH, May 23-25, 1989 (NASA TM-102050).
17. Gruber, R. P., "Power Electronics for a 1 kW Arcjet Thruster," AIAA Paper 86-1507, June 1986 (NASA TM-87340).
18. Boyle, M. J. and Jahn, R. G., "Acceleration Processes in the Quasi-Steady Magnetoplasma-dynamic Discharge," Report 1188, Princeton University, 1974.
19. Private Communication, Dr. Francis M. Curran, NASA Lewis Research Center, Cleveland, OH, June, 1989.
20. Kiel, R. E. and Gustafson, W. A., "Electrostatic Probe in a Collisionless Plasma," *The Physics of Fluids*, Vol. 9, No. 8, August, 1966, pp. 1531-1539.
21. Kiel, R. E., "Electrostatic Probe Theory for Free-Molecular Spheres," *AIAA Journal*, Vol. 9, No. 7, July, 1971, pp. 1380-1382.
22. Peterson, E. W. and Talbot, L., "Collisionless Electrostatic Single-Probe and Double-Probe Measurements," *AIAA Journal*, Vol. 8, No. 12, December, 1970, pp. 2215 - 2219.
22. Spitzer, L. Jr., *Physics of Fully Ionized Gases*, Interscience Publishers, Inc., New York, 1956.

TABLE I. - Estimates of Relevant Mean Free Paths for Langmuir Probe Operation

Assumptions:			
		$n_e \sim n_i$	
		$n_e \sim 5 \times 10^{-4} n_n$	
		$n_e$ ranges from $9 \times 10^7$ to $1 \times 10^{10}/\text{cm}^3$	
		$T_e$ ranges from 0.1 - 0.3 eV	
		$T_i \sim 0.1 T_e$	
<u>Collision Type</u>	$\lambda_{\min}$ ( cm )	$\lambda_{\max}$ ( cm )	<u>Notes</u>
ion - ion	$5 \times 10^{-2}$	$3 \times 10^1$	Based on Spitzer's relation <sup>11,22</sup>
ion-electron	$7 \times 10^3$	$4 \times 10^5$	Based on Spitzer's relation <sup>11,22</sup>
electron-electron	$3 \times 10^0$	$2 \times 10^2$	Based on Spitzer's relation <sup>11,22</sup>
electron-ion	$3 \times 10^0$	$2 \times 10^2$	$\lambda_{e-i} \sim \lambda_{e-e}$ <sup>11</sup>
neutral-neutral	$1 \times 10^1$	$1 \times 10^3$	Gas kinetic theory
ion-neutral	$3 \times 10^0$	$3 \times 10^2$	$\lambda_{i-n} \sim \lambda_{n-n}$ <sup>11</sup>
electron-neutral	$2 \times 10^1$	$4 \times 10^3$	$Q \sim 5 \times 10^{-8} \text{ cm}^3/\text{sec}$ <sup>4</sup>

TABLE II. - Major Thruster Components and Dimensions of Interest.

	<u>Thruster A</u>	<u>Thruster B</u>
Component Materials		
Anode Housing	Titaniated Zirconiated Molybdenum	Stainless Steel
Anode/Nozzle	2% Thoriated Tungsten	2% Thoriated Tungsten
Cathode	2% Thoriated Tungsten	2% Thoriated Tungsten
Injection Disk	Molybdenum	Molybdenum
Constrictor Geometry		
Constrictor Diameter, $D_c$ , cm	0.038	0.064
Constrictor Length, $L_c$ , cm	0.036	0.025
Arc Gap Setting, $G$ , cm	0.058	0.058
Nozzle Geometry		
Exit Diameter, cm	0.932	0.952
Throat Diameter, cm	0.038	0.064
Half Angle, deg	20°	20°
Area Ratio	600	220

Table III. - Typical Arcjet Thruster Operating Conditions and Performance Characteristics

<u>Thruster A ( <math>D_c = 0.038</math> cm )</u>				
Mixture Ratio of $N_2:H_2$	1:2	1:2	1:2	1:2
Total Mass Flow Rate, mg/s	35.7	35.7	23.8	23.8
Average Molecular Weight	10.6	10.6	10.6	10.6
Inlet Pressure, $N/m^2$	$6.9 \times 10^5$	$8.9 \times 10^5$	$6.0 \times 10^5$	$7.6 \times 10^5$
Arc Current, A	8.0	11.0	8.0	11.0
Arc Voltage, v	123.6	118.7	110.7	106.6
Arc Power, W	989	1305	885	1172
Power/Mass Flow Rate, kJ/g	27.7	36.6	37.2	49.2
Thrust, g	16.2	18.1	11.6	12.9
Specific Impulse, sec	455	506	486	541
Overall Efficiency, percent	35.1	33.1	30.9	28.2
Cold Flow Isp, sec	116	116	117	117
Cold Flow Thrust, g	4.2	4.2	2.8	2.8
<u>Thruster B ( <math>D_c = 0.064</math> cm )</u>				
Mixture Ratio of $N_2:H_2$	1:2	1:2	1:2	1:2
Total Mass Flow Rate, mg/s	49.7	49.7	40.7	40.7
Average Molecular Weight	10.6	10.6	10.6	10.6
Inlet Pressure, $N/m^2$	$3.93 \times 10^5$	$4.23 \times 10^5$	$3.41 \times 10^5$	$3.69 \times 10^5$
Arc Current, A	8.0	11.0	8.0	11.0
Arc Voltage, v	113.7	105.2	106.6	98.6
Arc Power, W	909	1158	852	1084
Power/Mass Flow Rate, kJ/g	18.3	23.3	20.9	26.6
Thrust, g	18.9	21.0	16.1	17.8
Specific Impulse, sec	380	422	396	436
Overall Efficiency, percent	36.7	35.8	35.0	33.6
Cold Flow Isp, sec	116	116	115	115
Cold Flow Thrust, g	5.8	5.8	4.7	4.7

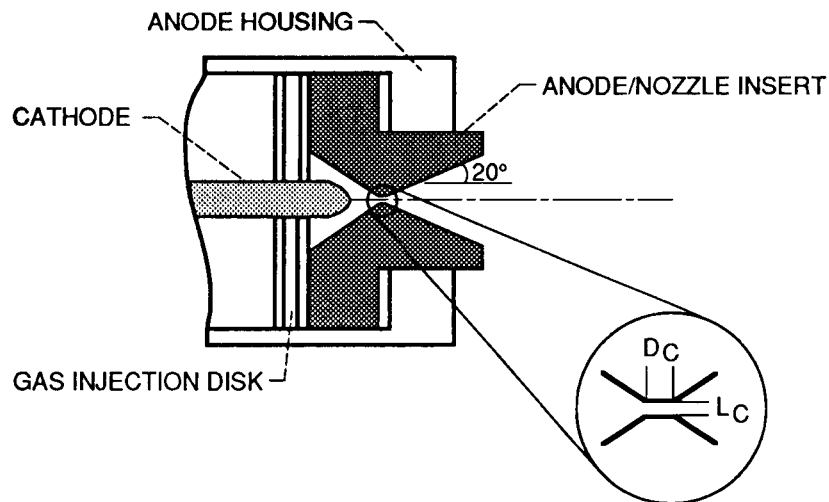


Figure 1. - Cross sectional schematic of arcjet thruster constrictor region.

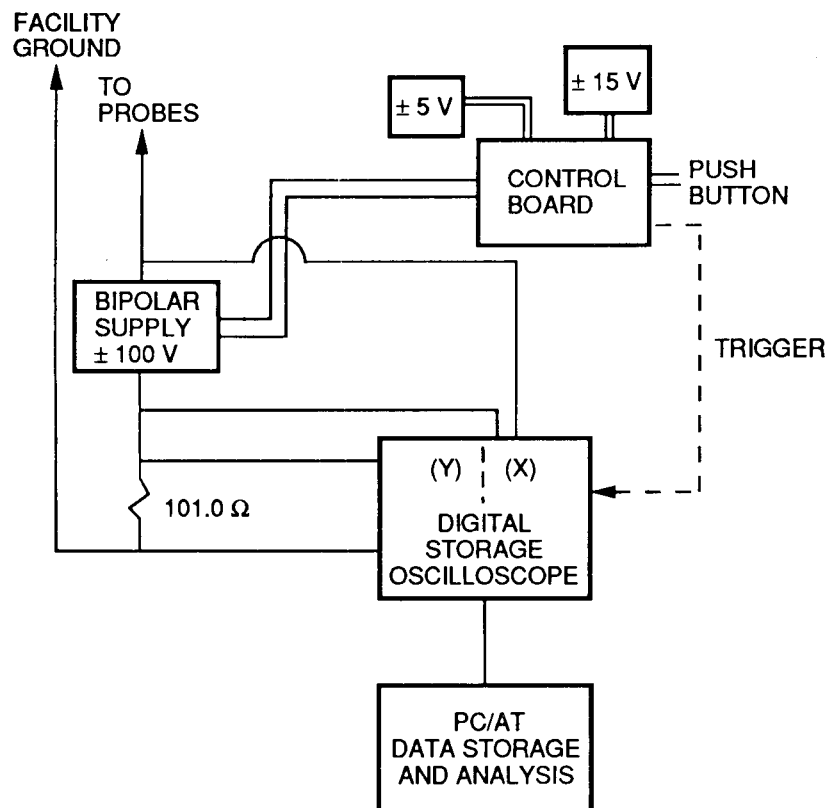


Figure 2. - Electrical schematic of Langmuir probe drive circuit and data acquisition.

ORIGINAL PAGE  
BLACK AND WHITE PHOTOGRAPH

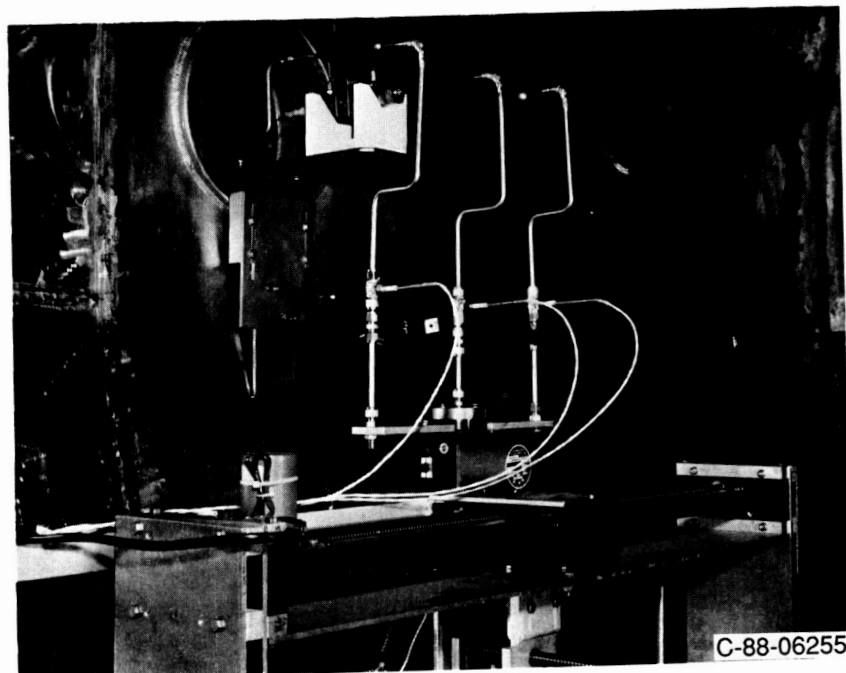
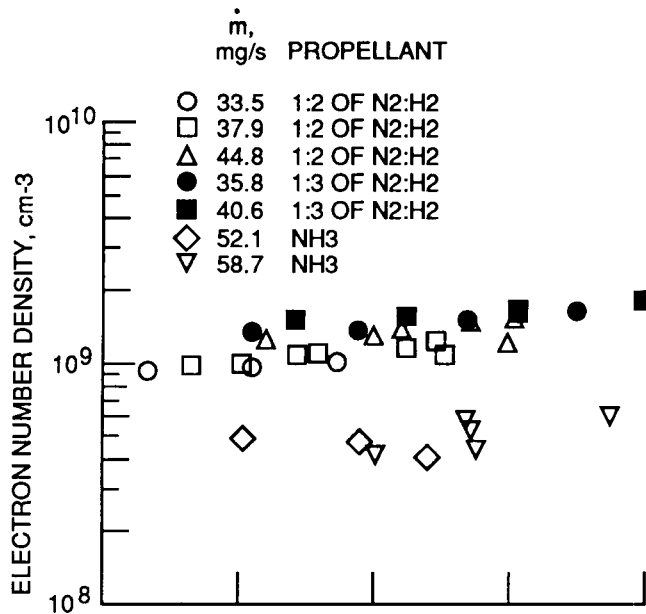
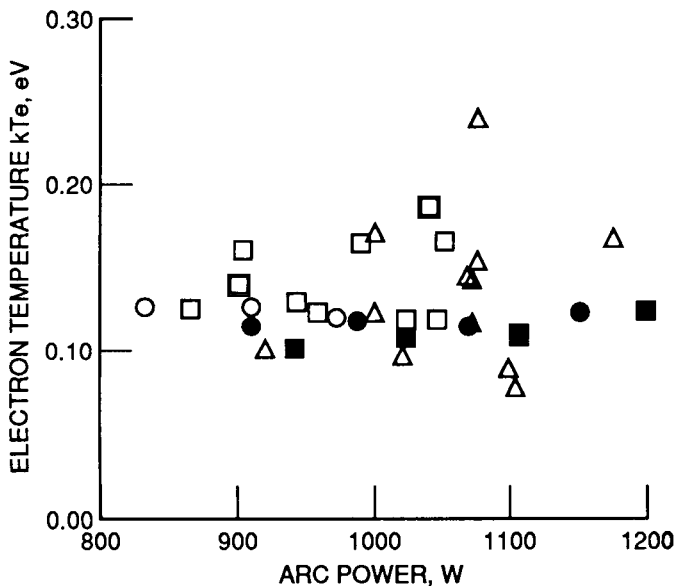


Figure 3. - Experimental configuration for plasma plume measurements in tank 5.

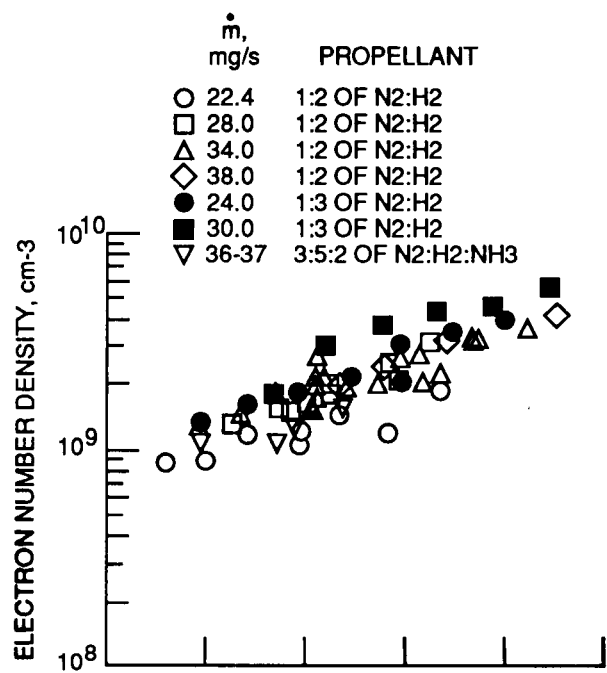


(a) Electron number density as a function of arc power.

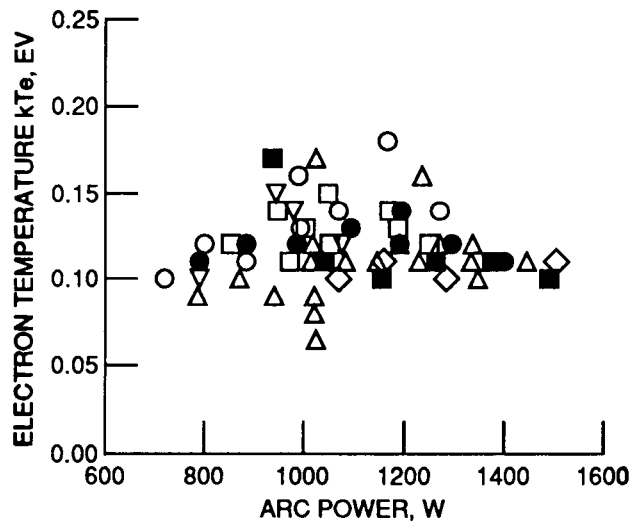


(b) Electron temperature as a function of arc power.

Figure 4. - Cumulative data for Thruster B ( $Z = 32$  cm; plume centerline).

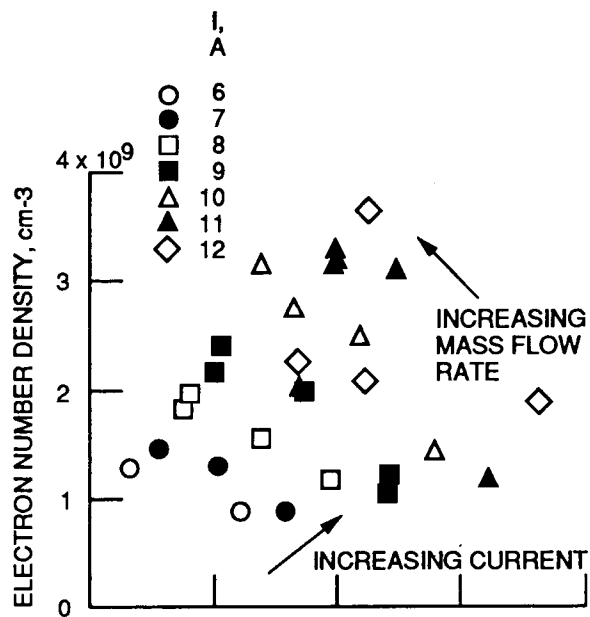


(a) Electron number density as a function of arc power.

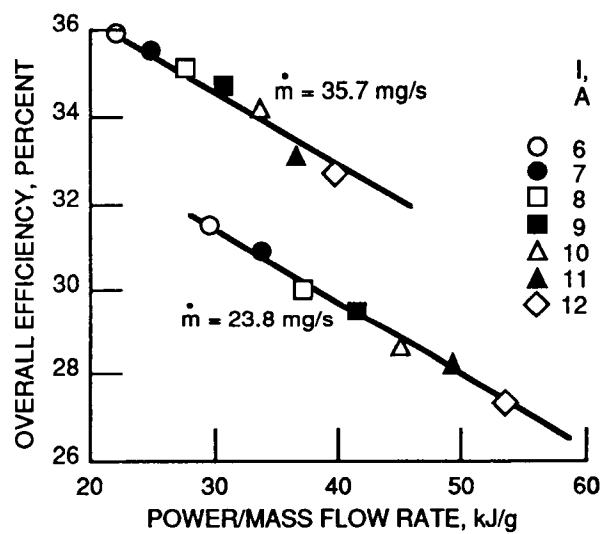


(b) Electron temperature as a function of arc power.

Figure 5. - Cumulative data for Thruster A ( $Z = 32$  cm; plume centerline).



(a) Electron number density as a function of power/mass flow rate.



(b) Thruster A performance data using 1:2 mixture.

Figure 6. - Plasma plume and performance characteristics of Thruster A (mixture ratio of  $N_2:H_2 = 1:2$ ).



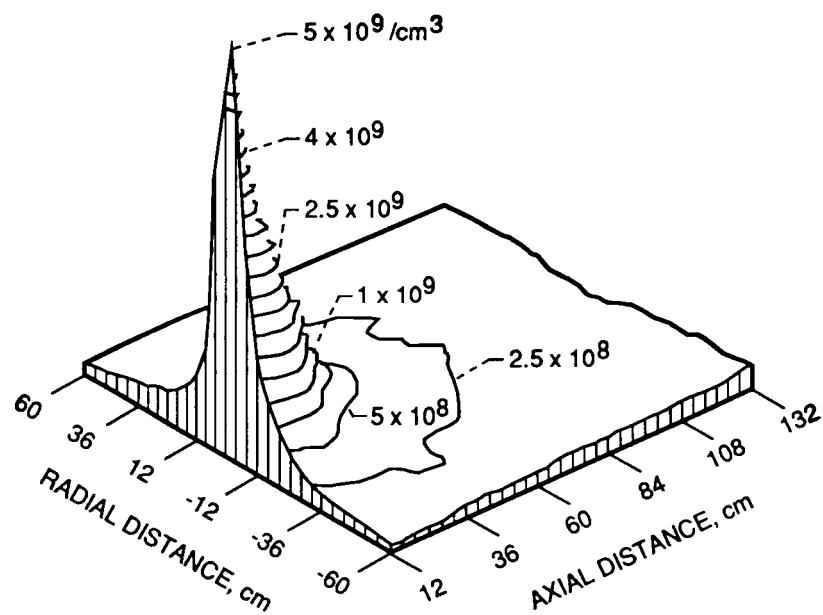
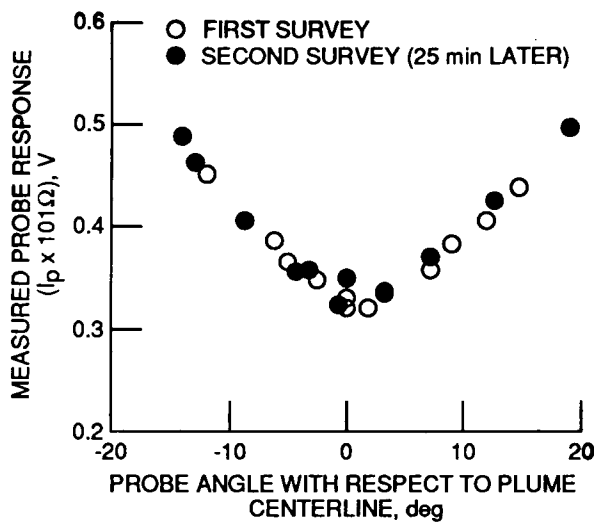
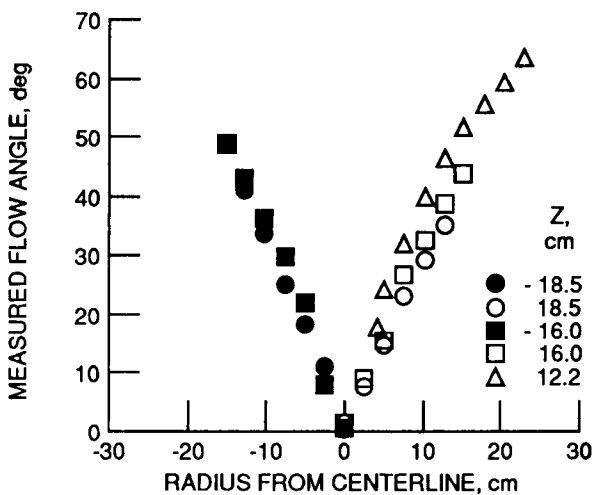


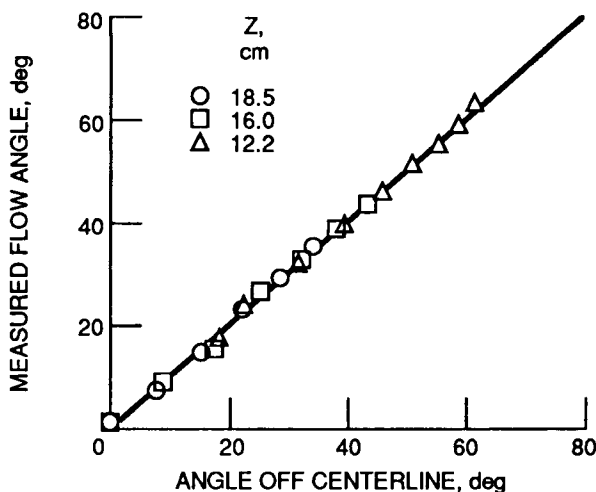
Figure 7. - Electron number density distribution in an arcjet thruster plume. Thruster B,  $I = 10$  A,  $\dot{m} = 43.4$  mg/s (1:2 mix).



(a) Measured probe voltage as a function of probe angle with respect to plume centerline.  $R = 0$  cm.

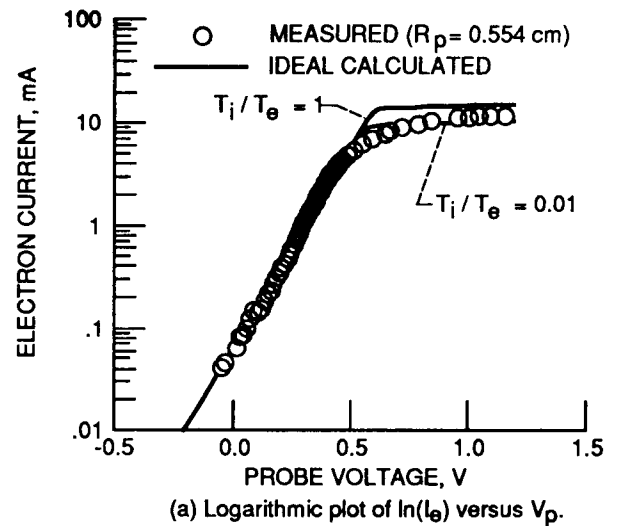


(b) Flow angle as a function of radial distance.

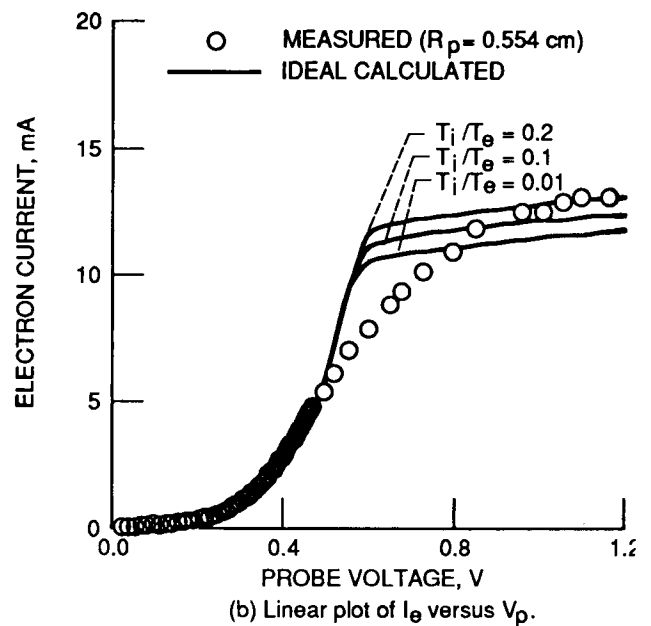


(c) Measured flow angle as a function of angle off centerline.

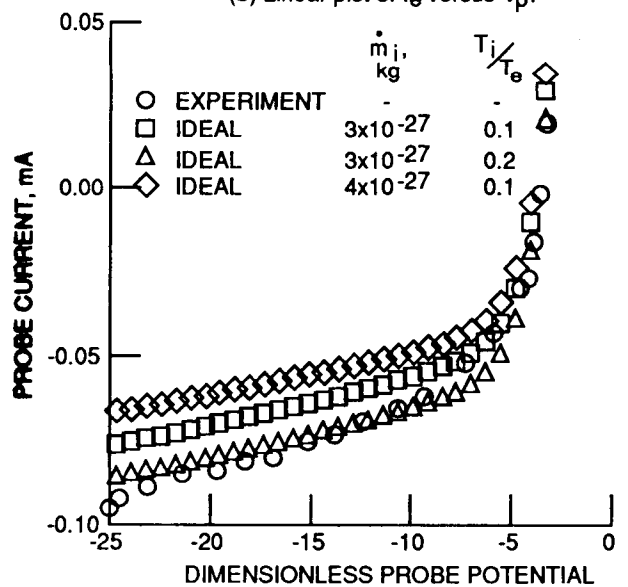
Figure 8. - Determination of flow angle using Langmuir probes.



(a) Logarithmic plot of  $\ln(I_e)$  versus  $V_p$ .



(b) Linear plot of  $I_e$  versus  $V_p$ .



(c) Total probe current collection as a function of dimensionless potential.

Figure 9. - Comparison of measured and calculated Langmuir probe response.

ORIGINAL PAGE  
BLACK AND WHITE PHOTOGRAPH

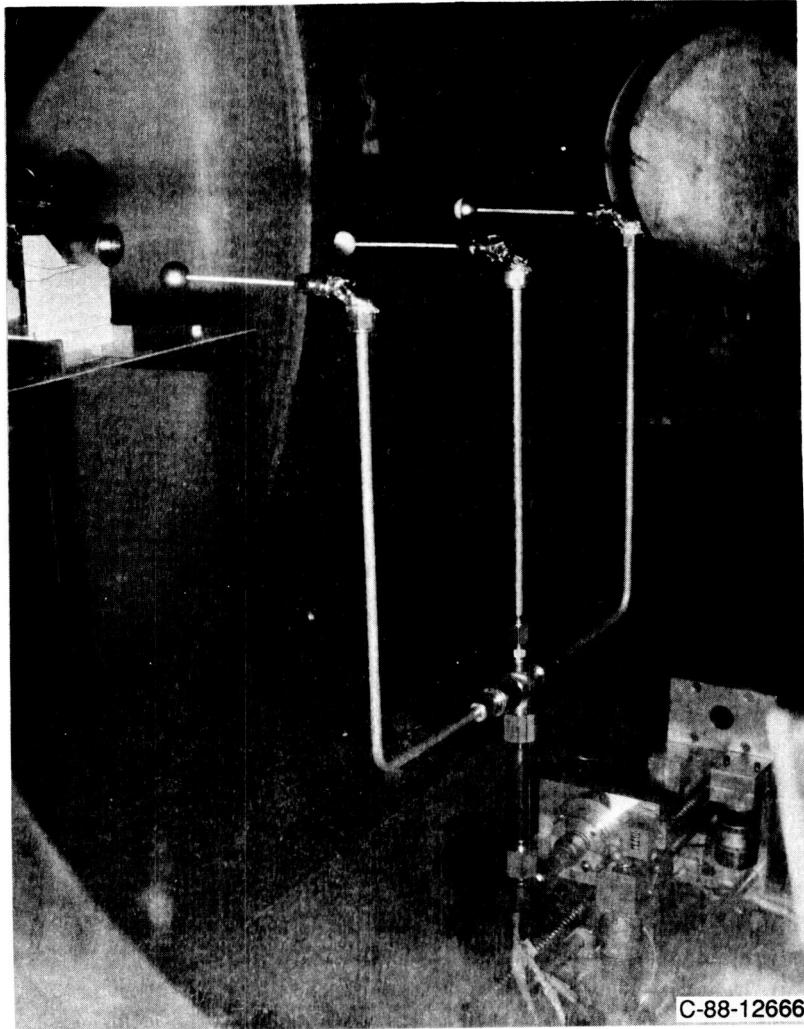


Figure 10. - Experimental configuration for effective probe area studies.

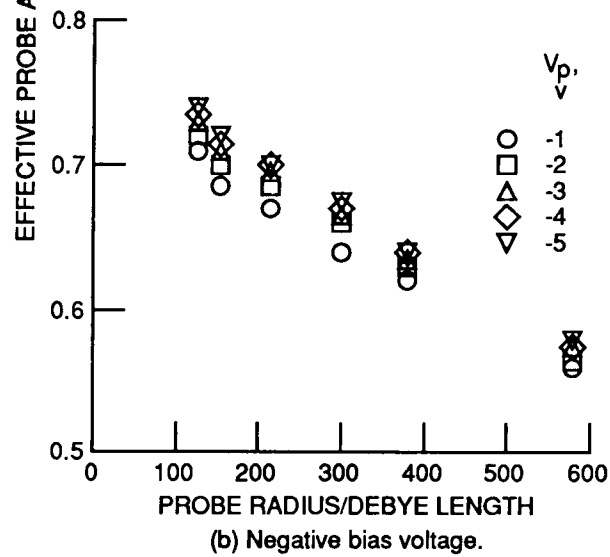
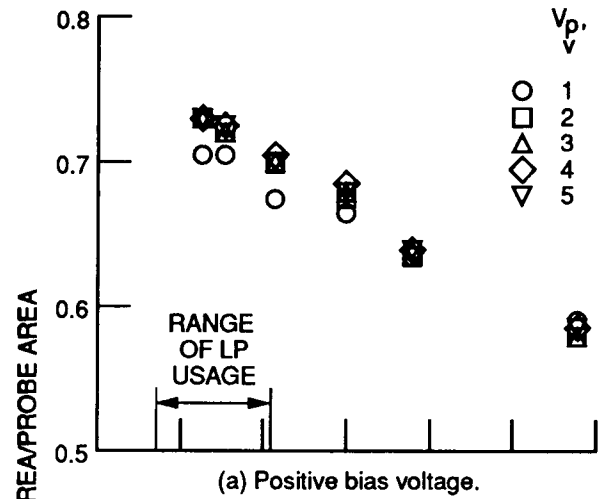


Figure 11. - Langmuir probe effective area as a function of probe radius/debye length.

# Report Documentation Page

1. Report No. NASA TM-102284 AIAA-89-2723		2. Government Accession No.		3. Recipient's Catalog No.	
4. Title and Subtitle  The Effects of Arcjet Operating Condition and Constrictor Geometry on the Plasma Plume				5. Report Date	
				6. Performing Organization Code	
7. Author(s)  Lynnette M. Carney and John M. Sankovic				8. Performing Organization Report No.  E-4877	
				10. Work Unit No.  506-42-31	
9. Performing Organization Name and Address  National Aeronautics and Space Administration Lewis Research Center Cleveland, Ohio 44135-3191				11. Contract or Grant No.	
				13. Type of Report and Period Covered  Technical Memorandum	
12. Sponsoring Agency Name and Address  National Aeronautics and Space Administration Washington, D.C. 20546-0001				14. Sponsoring Agency Code	
15. Supplementary Notes  Prepared for the 25th Joint Propulsion Conference cosponsored by the AIAA, ASME, SAE, and ASEE, Monterey, California, July 10-12, 1989. Lynnette M. Carney, NASA Lewis Research Center; John M. Sankovic, The University of Akron, Akron, Ohio 44325.					
16. Abstract  Measurements of plasma number density and electron temperature have been obtained in the plumes of laboratory arcjet thrusters using electrostatic probes of both spherical and cylindrical geometry. The two arcjet thrusters used in this investigation had different constrictor/nozzle geometries and operated on mixtures of nitrogen, hydrogen, and ammonia to simulate the decomposition products of hydrazine and ammonia. An increase in the measured electron number density was observed for both geometries with increasing arc power at a constant mass flow rate and with increasing mass flow rate at a constant arc current. For a given operating condition, the electron number density decreased exponentially off centerline and followed an inverse distance-squared relationship along the thrust axis. Typical measured electron temperatures ranged from 0.1 to 0.2 eV.					
17. Key Words (Suggested by Author(s))  Arcjet thrusters Plumes Electric propulsion Plasma diagnostics			18. Distribution Statement  Unclassified - Unlimited Subject Category 20		
19. Security Classif. (of this report)  Unclassified		20. Security Classif. (of this page)  Unclassified		21. No of pages  28	
				22. Price*  A03	